Practical Pulse-Shaping Waveforms for Reduced-Cyclic-Prefix OTFS

P. Raviteja, Yi Hong, Emanuele Viterbo, and Ezio Biglieri

***Abstract*—In this paper, we model $M \times N$ orthogonal time frequency space modulation (OTFS) over a P-path doubly dispersive channel with delays less than $\tau_{\max}$ and Doppler shifts in the range $(\nu_{\min}, \nu_{\max})$. We first derive in a simple matrix form the input–output relation in the delay-Doppler domain for practical (e.g., rectangular) pulse-shaping waveforms, next generalize it to arbitrary waveforms. This relation extends the original OTFS input–output approach, which assumes ideal pulse-shaping waveforms that are bi-orthogonal in both time and frequency. We show that the OTFS input–output relation has a simple sparse structure that enables one to use low-complexity detection algorithms. Different from previous work, only a single cyclic prefix is added at the end of the OTFS frame, significantly reducing the overhead, without incurring any penalty from the loss of bi-orthogonality of the pulse-shaping waveforms. Finally, we compare the OTFS performance with different pulse-shaping waveforms, and show that the reduction of out-of-band power may introduce nonuniform channel gains for the transmitted symbols, thus impairing the overall error performance.**

***Index Terms*—OTFS, circulant matrices, delay-Doppler domain.**

I. Introduction

Orthogonal time frequency space (OTFS) modulation has been recently proposed in [1], [3] to efficiently address the high Doppler sensitivity problem occurring in orthogonal frequency division multiplexing (OFDM) modulation. The key idea of OTFS is to transmit the information symbols in the delay–Doppler plane rather than in the time–frequency plane as with OFDM. The delay–Doppler plane captures the delays and Doppler shifts of the physical paths present in the wireless channel, and allows a sparse representation of the channel.

While [1], [3] present an overall system level description of OTFS, exact implementation details were not provided. Moreover, the relations in [1], [3] assume ideal pulse-shaping waveforms that satisfy orthogonality conditions in both time and frequency, which is not practically feasible due to Heisenberg's uncertainty principle. Several other works ([5]–[9] and references therein) propose an *OFDM-based OTFS system*, where non-ideal rectangular pulse-shaping waveforms and cyclic prefix (CP) for every OFDM symbol in OTFS frame are considered. However, it is non-trivial to extend their input–output relations to the case of arbitrary practical OTFS waveforms.

On the other hand, many works focused on the design of waveforms that are close to ideal waveforms in the context of pulse-shaped OFDM (PS-OFDM) [10]–[12]. The objective of these works is to analyze and reduce interferences, i.e., inter-carrier and inter-symbol interferences, that occur in PS-OFDM due to non-orthogonality of waveforms. However, in this paper, we show that the channel relations in OTFS for practical non-orthogonal waveforms follow a simple sparse structure, enabling the use of low-complexity detection algorithms.

Inspired by a simple matrix representation of OFDM systems using circulant-matrix decomposition, in this work, we first express the OTFS effective channel transfer matrix using two matrix decompositions, one for delay and another for Doppler components. Next, we simplify the OTFS effective channel by applying some properties of block circulant matrices, and show that the effective channel transfer matrix has a simple sparse structure, with a sparsity level depending on the number of paths in the channel. Thanks to the sparse matrix structure, a low-complexity detection algorithm can be used at the receiver. Moreover, we show how our approach can be easily extended to *arbitrary practical pulse-shaping waveforms* that are applied to the time domain signal. Further, we compare the OTFS performance of rectangular and prolate spheroidal waveforms, and illustrate a tradeoff between out-of-band radiation and BER performance.

We use the following notation throughout the paper. We let a, $\mathbf{a}$, and $\mathbf{A}$ represent scalar, vector, and matrix, respectively. The terms $a(n)$ and $\mathbf{A}(m,n)$ represent the nth element of $\mathbf{a}$ and (m,n)th element of $\mathbf{A}$. Notations $\mathbf{A}^{\mathrm{H}}$ and $\mathbf{A}^n$ represent the Hermitian transpose and the nth power of $\mathbf{A}$. Notation $\mathbb{C}^{M\times N}$ denotes the set of $M \times N$ dimensional matrices with each entry from the complex plane. Let $\otimes$ be the Kronecker product and $\mathbf{A} = \mathrm{diag}[\mathbf{A}_0, \ldots, \mathbf{A}_{N-1}] \in \mathbb{C}^{MN\times MN}$ the block diagonal matrix with $\{\mathbf{A}_0, \ldots, \mathbf{A}_{N-1}\} \in \mathbb{C}^{M\times M}$ as diagonal blocks. Finally, we let $\mathbf{F}_n = \{\frac{1}{\sqrt{n}} e^{2\pi jkl/n}\}_{k,l=0}^{n-1}$ and $\mathbf{F}_n^{\mathrm{H}}$ be the n-point DFT and the IDFT matrices, and the term $\mathbf{I}_M$ be a M-dimensional identity matrix.

II. System Model

In this section, we describe the OTFS system using matrix notations. We assume that the total duration of the transmitted signal frame is NT and the sampling interval is T/M. Moreover, we let $g_{\mathrm{tx}}(t)$ and $g_{\mathrm{rx}}(t)$ denote a pulse of duration $[0, T]$ repeated N times in the frame.

A. Transmitter

Let $\mathbf{X} \in \mathbb{C}^{M\times N}$ denote the two-dimensional information symbols transmitted in the delay–Doppler plane. To convert these symbols to time–frequency signals, Inverse Symplectic Fast Fourier Transform (ISFFT) precoding is applied (this amounts to an M-point FFT of the columns and an N-point IFFT of the rows of $\mathbf{X}$). The "Heisenberg transform modulator" generates the time domain signal using an M-point IFFT along with the pulse-shaping waveform $g_{\mathrm{tx}}(t)$. The

Manuscript received June 4, 2018; revised September 8, 2018; accepted October 26, 2018. Date of publication October 31, 2018; date of current version January 15, 2019. The work of the first three authors was supported by the Australian Research Council through the Discovery Project under Grant DP160100528. The work of Ezio Biglieri was supported by the Spanish Ministry of Economy and Competitiveness under Grant TEC2015-66228-P MINECO/FEDER, UE. The review of this paper was coordinated by Prof. Y. T. Su. *(Corresponding author: Emanuele Viterbo.)*

P. Raviteja, Y. Hong, and E. Viterbo are with the ECSE Department, Monash University, Clayton, VIC 3800, Australia (e-mail: raviteja.patchava@monash.edu; yi.hong@monash.edu; emanuele.viterbo@monash.edu).

E. Biglieri is with the Universitat Pompeu Fabra, Barcelona 08002, Spain (e-mail: e.biglieri@ieee.org).

Color versions of one or more of the figures in this paper are available online at http://ieeexplore.ieee.org.

Digital Object Identifier 10.1109/TVT.2018.2878891

transmitted signal can be written as [5]

$$\mathbf{S} = \mathbf{G}_{\rm tx}\mathbf{F}_M^{\rm H}(\mathbf{F}_M\,\mathbf{X}\mathbf{F}_N^{\rm H}) = \mathbf{G}_{\rm tx}\mathbf{X}\mathbf{F}_N^{\rm H} \tag{1}$$

where the diagonal matrix $\mathbf{G}_{\rm tx}$ has the samples of $g_{\rm tx}(t)$ as its entries: $\mathbf{G}_{\rm tx} = {\rm diag}[g_{\rm tx}(0), g_{\rm tx}(T/M), \ldots, g_{\rm tx}((M-1)T/M)] \in \mathbb{C}^{M\times M}$ (for rectangular waveforms, $\mathbf{G}_{\rm tx}$ reduces to the identity matrix $\mathbf{I}_M$). Column-wise vectorization of the $M \times N$ matrix $\mathbf{S}$ in (1) yields the $MN \times 1$ vector

$$\mathbf{s} = {\rm vec}(\mathbf{S}) = (\mathbf{F}_N^{\rm H} \otimes \mathbf{G}_{\rm tx})\mathbf{x} \tag{2}$$

where $\mathbf{x} = {\rm vec}(\mathbf{X})$ and denoting by $\otimes$ the Hadamard product. We assume that a cyclic prefix (CP) of length $L-1$ (see after (5)) is appended to $\mathbf{s}$ before transmission.

Note that we assume only one CP for the entire OTFS frame, whereas the other works [5]–[9] considered N CP's for one OTFS frame. This design assumption considerably increases the spectral efficiency of the overall system, particularly for the cases where the value of N is large, (e.g., 64, 128) or the CP overhead is large (e.g., 802.11ac requires 25% CP).

B. Channel

After parallel-to-serial and digital-to-analog conversion, denoting by $s(t)$ the transmitted signal, the received signal $r(t)$ can be expressed in the form [1], [2]

$$r(t) = \int\int h(\tau,\nu)s(t-\tau)e^{j2\pi\nu(t-\tau)}d\tau d\nu + w(t). \tag{3}$$

Since typically there is only a small number of reflectors in the channel with associated delays and Doppler shifts, very few parameters are often needed to model the channel in the delay–Doppler domain. Given the sparsity of the channel representation, it is convenient to express the response $h(\tau,\nu)$ in the form

$$h(\tau,\nu) = \sum_{i=1}^{P} h_i\delta(\tau-\tau_i)\delta(\nu-\nu_i) \tag{4}$$

where $\delta(\cdot)$ is the Dirac delta function, P is the number of propagation paths, and h_i, τ_i, and ν_i denote the complex path gain, delay, and Doppler shift (or frequency) associated with the i-th path, respectively. The delay and Doppler-shift taps for i-th path are given by

$$\tau_i = \frac{l_i}{M\Delta f},\quad \nu_i = \frac{k_i}{NT} \tag{5}$$

For ease of derivations, we assume the delay and Doppler shifts as integer multiples of $\frac{1}{M\Delta f}$ and $\frac{1}{NT}$, respectively, i.e., we assume l_i, k_i are integers. However, fractional delay and Doppler shifts can also be handled using the techniques discussed in [4] and [16] by adding virtual integer taps in the delay–Doppler channel. Hence, the results derived in this paper can be straightforwardly extend to the fractional delay and Doppler shifts.

Here, NT and $M\Delta f$ denote the total duration and bandwidth of the transmitted signal frame, respectively. Throughout the paper, we have considered $T\Delta f = 1$, i.e., OTFS is critically sampled for all pulse-shaping waveforms. We assume that the maximum delay of the channel is $\tau_{\max} = (L-1)T/M$, i.e., $\max(l_i) = L-1$. Moreover, $l_i < M$ and $k_i < N$ (i.e., the channel is underspread: for example, typical values of l_i and k_i in LTE channels are less than 10% of M and N, respectively). The received signal $y(t)$ is sampled at a rate $f_s = M\Delta f = M/T$ and, after discarding the CP, a vector $\mathbf{r} = \{r(n)\}_{n=0}^{MN-1}$ is formed, whose entries, from (3) and (4), are the samples

$$r(n) = \sum_{i=1}^{P} h_i e^{j2\pi\frac{k_i(n-l_i)}{MN}} s([n-l_i]_{MN}) + w(n) \tag{6}$$

where $[\cdot]_n$ denotes mod-n operation. We write (6) in vector form as

$$\mathbf{r} = \mathbf{H}\mathbf{s} + \mathbf{w}, \tag{7}$$

where $\mathbf{H}$ is the $MN \times MN$ matrix

$$\mathbf{H} = \sum_{i=1}^{P} h_i\mathbf{\Pi}^{l_i}\mathbf{\Delta}^{k_i}, \tag{8}$$

with $\mathbf{\Pi}$ the permutation matrix (forward cyclic shift),

$$\mathbf{\Pi} = \begin{bmatrix} 0 & \cdots & 0 & 1 \\ 1 & \ddots & 0 & 0 \\ \vdots & \ddots & \ddots & \vdots \\ 0 & \cdots & 1 & 0 \end{bmatrix}_{MN\times MN} \tag{9}$$

and $\mathbf{\Delta}$ is the $MN \times MN$ diagonal matrix

$$\mathbf{\Delta} = {\rm diag}\left[z^0, z^1, \ldots, z^{MN-1}\right] \tag{10}$$

with $z = e^{\frac{j2\pi}{MN}}$. Here, the matrices $\mathbf{\Pi}$ and $\mathbf{\Delta}$ model the delays and the Doppler shifts in (3), respectively. Each path introduces an l_i-step cyclic shift of the transmitted signal vector $\mathbf{s}$, modeled by $\mathbf{\Pi}^{l_i}$, and modulates it with a carrier at frequency k_i, modeled by $\mathbf{\Delta}^{k_i}$.

C. Receiver

At the receiver, we invert the transmitter operations to transform the received signal samples $\mathbf{r}$ into the time–frequency domain symbols $\mathbf{R} = {\rm vec}^{-1}(\mathbf{r})$ (the vector elements are folded back into a matrix), next into the delay–Doppler domain symbols $\mathbf{Y} = \mathbf{F}_M^{\rm H}(\mathbf{F}_M\,\mathbf{G}_{\rm rx}\mathbf{R})\mathbf{F}_N$. To do this, we apply an M-point FFT followed by an SFFT. Here, $\mathbf{G}_{\rm rx} \in \mathbb{C}^{M\times M}$ represents the filter operating at the receiver and using the pulse-shaping waveform $g_{\rm rx}(t)$. We can write $\mathbf{G}_{\rm rx} = {\rm diag}[g_{\rm rx}(0), g_{\rm rx}(T/M), \ldots, g_{\rm rx}((M-1)T/M)]$.

In vectorized form the received signal in the delay–Doppler domain can be written, after substituting (2) in (7), as

$$\begin{aligned}\mathbf{y} &= (\mathbf{F}_N \otimes \mathbf{G}_{\rm rx})\mathbf{r} \\ &= (\mathbf{F}_N \otimes \mathbf{G}_{\rm rx})\mathbf{H}(\mathbf{F}_N^{\rm H} \otimes \mathbf{G}_{\rm tx})\mathbf{x} + (\mathbf{F}_N \otimes \mathbf{G}_{\rm rx})\mathbf{w} \\ &= \mathbf{H}_{\rm eff}\mathbf{x} + \widetilde{\mathbf{w}}\end{aligned} \tag{11}$$

where $\mathbf{H}_{\rm eff} = (\mathbf{F}_N \otimes \mathbf{G}_{\rm rx})\mathbf{H}(\mathbf{F}_N^{\rm H} \otimes \mathbf{G}_{\rm tx})$ denotes the effective channel matrix, and $\widetilde{\mathbf{w}} = (\mathbf{F}_N \otimes \mathbf{G}_{\rm rx})\mathbf{w}$ the noise vector. It can be easily seen that in general $\widetilde{\mathbf{w}}$ has a diagonal covariance matrix, which becomes a scalar matrix (indicating iid noise samples) in the case of rectangular waveforms, i.e., $\mathbf{G}_{\rm rx} = \mathbf{I}_M$.

In the next section, we will simplify $\mathbf{H}_{\rm eff}$ to obtain a simple relation between the input and output symbols in delay–Doppler domain.

III. Input–Output Relation

In this section, we first derive the simplified form of $\mathbf{H}_{\text{eff}}$ for the rectangular waveforms and then extend that relation to the arbitrary waveforms at the transmitter and receiver. For the rectangular waveforms, both $\mathbf{G}_{\text{tx}}$ and $\mathbf{G}_{\text{rx}}$ are equal to $\mathbf{I}_M$, and hence

$$\mathbf{H}_{\text{eff}}^{\text{rect}} = (\mathbf{F}_N \otimes \mathbf{I}_M)\mathbf{H}(\mathbf{F}_N^{\text{H}} \otimes \mathbf{I}_M). \tag{13}$$

Let us first recall the following lemma on circulant matrices decomposition [13].

Lemma 1: Let $\mathbf{A} = \text{circ}[\mathbf{A}_0, \ldots, \mathbf{A}_{N-1}]$ denote the $MN \times MN$ block-circulant matrix

$$\mathbf{A} = \begin{bmatrix} \mathbf{A}_0 & \mathbf{A}_{N-1} & \cdots & \mathbf{A}_1 \\ \mathbf{A}_1 & \mathbf{A}_0 & \cdots & \mathbf{A}_2 \\ \vdots & \ddots & \ddots & \vdots \\ \mathbf{A}_{N-1} & \mathbf{A}_{N-2} & \cdots & \mathbf{A}_0 \end{bmatrix} \tag{14}$$

where $\mathbf{A}_0, \ldots, \mathbf{A}_{N-1}$ are square matrices of order M. Then $\mathbf{A}$ can be block-diagonalized in the following forms:

$$\mathbf{A} = (\mathbf{F}_N^{\text{H}} \otimes \mathbf{I}_M)\mathbf{D}(\mathbf{F}_N \otimes \mathbf{I}_M) \tag{15}$$

$$= (\mathbf{F}_N \otimes \mathbf{I}_M)\widetilde{\mathbf{D}}(\mathbf{F}_N^{\text{H}} \otimes \mathbf{I}_M) \tag{16}$$

where $\mathbf{D}$ and $\widetilde{\mathbf{D}}$ are the block diagonal matrices

$$\mathbf{D} = \text{diag}\,[\mathbf{D}_0, \mathbf{D}_1, \ldots, \mathbf{D}_{N-1}]$$
$$\widetilde{\mathbf{D}} = \text{diag}\left[\widetilde{\mathbf{D}}_0, \widetilde{\mathbf{D}}_1, \ldots, \widetilde{\mathbf{D}}_{N-1}\right] \tag{17}$$

with block submatrices $\mathbf{D}_0, \ldots, \mathbf{D}_{N-1}, \widetilde{\mathbf{D}}_0, \ldots, \widetilde{\mathbf{D}}_{N-1} \in \mathbb{C}^{M\times M}$. The (i,j)-th entry ($0 \le i \le M-1, 0 \le j \le M-1$) of $\mathbf{D}_n$ ($0 \le n \le N-1$) can be computed as the nth element of the DFT of the vector $\mathbf{a}^{(i,j)} = [\mathbf{A}_0(i,j), \ldots, \mathbf{A}_{N-1}(i,j)]^T$, i.e.,

$$[\mathbf{D}_0(i,j), \ldots, \mathbf{D}_{N-1}(i,j)]^T = \sqrt{N}\mathbf{F}_N\,\mathbf{a}^{(i,j)} \tag{18}$$

Similar to $\mathbf{D}$, $\widetilde{\mathbf{D}}$ is related to $\mathbf{a}^{(i,j)}$ by

$$\left[\widetilde{\mathbf{D}}_0(i,j), \ldots, \widetilde{\mathbf{D}}_{N-1}(i,j)\right]^T = \sqrt{N}\mathbf{F}_N^{\text{H}}\,\mathbf{a}^{(i,j)}.$$

The above can also be expressed in the form

$$\mathbf{a}^{(i,j)} = \frac{1}{\sqrt{N}}\mathbf{F}_N\left[\widetilde{\mathbf{D}}_0(i,j), \ldots, \widetilde{\mathbf{D}}_{N-1}(i,j)\right]^T \tag{19}$$

Proof: See [13] for the details. The proof of (18) is based on the fact that the $N \times N$ submatrices of $\mathbf{A}$ obtained by taking a row and a column every M are circulant. There are M^2 distinct such circulant submatrices. ■

The following theorem yields a simplified form of $\mathbf{H}_{\text{eff}}$.

Theorem 1: The effective channel matrix $\mathbf{H}_{\text{eff}}$ for rectangular waveforms can be written as

$$\mathbf{H}_{\text{eff}}^{\text{rect}} = \sum_{i=1}^{P} h_i \mathbf{T}^{(i)}, \tag{20}$$

where the entry (p,q), $0 \le p \le MN-1, 0 \le q \le MN-1$, of $\mathbf{T}^{(i)}$ is shown in (12) at the bottom of the page. In (12), the values of n and m can be computed from $p = (m,n)$ using $n = \lfloor \frac{p}{M} \rfloor$ and $m = p - nM$. Notice that $\mathbf{H}_{\text{eff}}^{\text{rect}}$ has only P nonzero entries in each row and column. The row and column entries describe the effect of information symbols on a particular received signal.

Proof: From (11), since $(\mathbf{F}_N \otimes \mathbf{I}_M)$ is a unitary matrix, the effective channel matrix can be written as

$$\mathbf{H}_{\text{eff}}^{\text{rect}} = \sum_{i=1}^{P} h_i \underbrace{\left[(\mathbf{F}_N \otimes \mathbf{I}_M)\mathbf{\Pi}^{l_i}(\mathbf{F}_N^{\text{H}} \otimes \mathbf{I}_M)\right]}_{\mathbf{P}^{(i)}}$$
$$\cdot \underbrace{\left[(\mathbf{F}_N \otimes \mathbf{I}_M)\mathbf{\Delta}^{k_i}(\mathbf{F}_N^{\text{H}} \otimes \mathbf{I}_M)\right]}_{\mathbf{Q}^{(i)}} = \sum_{i=1}^{P} h_i \mathbf{P}^{(i)}\mathbf{Q}^{(i)} \tag{21}$$

(a) Evaluation of $\mathbf{P}^{(i)}$ – Since $\mathbf{\Pi}$ is a permutation matrix, $\mathbf{\Pi}^{l_i}$ is also a permutation matrix with 1s in $(p, [p-l_i]_{MN})$th entries, for $0 \le p \le MN-1$, and zeros elsewhere. Further, $\mathbf{\Pi}^{l_i}$ is a circulant matrix which can also be seen as block-circulant with the form (14), in which $\mathbf{A}_n = \mathbf{\Pi}_n^{l_i}$ for $n = 0, \ldots, N-1$. Therefore, application of Lemma 1 shows that $\mathbf{P}^{(i)}$ has the block-diagonal form (17), with $N \times N$ diagonal blocks denoted by $\mathbf{P}_0^{(i)}, \ldots, \mathbf{P}_{N-1}^{(i)}$.

Since $l_i < M$, $\mathbf{\Pi}_2^{l_i}, \ldots, \mathbf{\Pi}_{N-1}^{l_i}$ are all-zero matrices ($\mathbf{0}$), and $\mathbf{\Pi}_0^{l_i}$ and $\mathbf{\Pi}_1^{l_i}$ has 1s in rows from l_i to $M-1$ and 0 to $l_i - 1$, respectively and all zeros in the remaining rows. Therefore, applying (18) in Lemma 1, and considering that the vector $\mathbf{a}(u,v)$ has only one nonzero element (which equals to 1), we obtain

$$\mathbf{P}_n^{(i)}(u,v) = \begin{cases} 1 & \text{if } u \ge l_i \text{ and } v = u - l_i \\ e^{-j2\pi\frac{n}{N}} & \text{if } u < l_i \text{ and } v = [u-l_i]_M \\ 0 & \text{otherwise} \end{cases} \tag{22}$$

for $0 \le n \le N-1$ and $0 \le u, v \le N-1$. Here, we obtain the values 1 and $e^{-j2\pi\frac{n}{N}}$ by applying the DFT to vectors $\mathbf{a} = [1, 0, \ldots, 0]^T$ and its cyclic shifts by n, respectively.

Finally, the (p,q)th entry of $\mathbf{P}^{(i)}$ for $0 \le p, q \le MN-1$ is

$$\mathbf{P}^{(i)}(p,q) = \begin{cases} 1 & \text{if } m \ge l_i, q = [m-l_i]_M + nM \\ e^{-j2\pi\frac{n}{N}} & \text{if } m < l_i, q = [m-l_i]_M + nM \\ 0 & \text{otherwise} \end{cases} \tag{23}$$

$$\mathbf{T}^{(i)}(p,q) = \begin{cases} e^{-j2\pi\frac{n}{N}} z^{k_i([m-l_i]_M)}, & \text{if } q = [m-l_i]_M + M[n-k_i]_N \text{ and } m < l_i \\ z^{k_i([m-l_i]_M)}, & \text{if } q = [m-l_i]_M + M[n-k_i]_N \text{ and } m \ge l_i \\ 0, & \text{otherwise.} \end{cases} \tag{12}$$

where, $n = \lfloor \frac{p}{M} \rfloor$ and $m = p - nM$. The values in (23) are obtained from (22) with the substitutions $p = nM + u, q = nM + v$ and $u = m$.

(b) Evaluation of $\mathbf{Q}^{(i)}$ – Observing that the diagonal matrix $\mathbf{\Delta}^{k_i}$ can be viewed as a block-diagonal matrix, and using (16), we can easily see that $\mathbf{Q}^{(i)}$ is a block-circulant matrix of the form (14).

Since the $M \times M$ blocks $\mathbf{\Delta}_0^{k_i}, \ldots, \mathbf{\Delta}_{N-1}^{k_i}$ are diagonal, from (19) we have

$$\mathbf{Q}_n^{(i)}(u,v) = 0, \text{ for } u \neq v, \ 0 \leq n \leq N-1 \tag{24}$$

and the diagonal entries of $\mathbf{Q}_0^{(i)}, \ldots, \mathbf{Q}_{N-1}^{(i)}$ are related to the elements of $\mathbf{\Delta}^{(i)}$ as

$$\begin{aligned}
&\left[\mathbf{Q}_0^{(i)}(u,u), \ldots, \mathbf{Q}_{N-1}^{(i)}(u,u)\right]^T \\
&= \left(\frac{1}{\sqrt{N}}\right) \mathbf{F}_N \left[\mathbf{\Delta}_0^{k_i}(u,u), \ldots, \mathbf{\Delta}_{N-1}^{k_i}(u,u)\right]^T \\
&= \left(\frac{1}{\sqrt{N}}\right) \mathbf{F}_N \left[z^{k_i u}, \ldots, z^{k_i(M(N-1)+u)}\right]^T \\
&= z^{k_i u}[0, \ldots, \underbrace{1}_{(k_i+1)^{th} \text{ entry}}, 0, \ldots, 0]^T
\end{aligned} \tag{25}$$

Therefore, we can write $\mathbf{Q}_n^{(i)}$ as

$$\mathbf{Q}_n^{(i)}(u,v) = \begin{cases} z^{k_i u} & \text{if } n = k_i \text{ and } u = v \\ 0 & \text{otherwise} \end{cases} \tag{26}$$

for $0 \leq n \leq N-1$ and $0 \leq u, v \leq N-1$. Further, the (p,q)th entry of $\mathbf{Q}^{(i)}$, for $0 \leq p, q \leq MN-1$, is equal to

$$\mathbf{Q}^{(i)}(p,q) = \begin{cases} z^{k_i m'} & \text{if } p = m' + M[n' + k_i]_N \\ 0 & \text{otherwise} \end{cases} \tag{27}$$

where, $n' = \lfloor \frac{q}{M} \rfloor$ and $m' = q - n'M$.

Now, the (p,q)th entry of $\mathbf{T}^{(i)} = \mathbf{P}^{(i)}\mathbf{Q}^{(i)}$, for $0 \leq p, q \leq MN-1$, can be written as

$$\mathbf{T}^{(i)}(p,q) = \sum_{e=0}^{MN-1} \mathbf{P}^{(i)}(p,e)\mathbf{Q}^{(i)}(e,q) \tag{28}$$

From (23), (27), and (28), we can see that $\mathbf{T}^{(i)}(p,q)$ has nonzero value only for

$$[m - l_i]_M + nM = m' + M[n' + k_i]_N, \tag{29}$$

which implies $m' = [m - l_i]_M$ and $n' = [n - k_i]_N$, or $q = [m - l_i]_M + M[n - k_i]_N$. Moreover, the value at $\mathbf{T}^{(i)}(p,q)$ depends on m and it is equal to $e^{-j2\pi n/N} z^{k_i([m-l_i]_M)}$ and $z^{k_i([m-l_i]_M)}$ for $m < l_i$ and $m \geq l_i$, respectively.

Finally, from (21) and (12), we see that there exists only one nonzero element in each row of $\mathbf{T}^{(i)}$. Further, based on the assumption that in different paths at least one of the k_i or l_i is also different, exactly P nonzero elements exist in each row and column of $\mathbf{H}_{\text{eff}}^{\text{rect}}$. ■

Example: Let us consider $M = 2, N = 2$, and examine $\mathbf{T}^{(i)}$ in the following four channel cases.

1) $k_1 = 0, l_1 = 0$*:* In this case, $\mathbf{P}^{(1)}$ and $\mathbf{Q}^{(1)}$ becomes $\mathbf{I}_4$ that leads $\mathbf{T}^{(1)}$ to $\mathbf{I}_4$. That is, the channel with zero delay and Doppler corresponds to a narrowband channel in OTFS.

2) $k_2 = 0, l_2 = 1$*:* In this case, $\mathbf{Q}^{(2)}$ becomes $\mathbf{I}_4$ and

$$\mathbf{P}^{(2)} = \mathbf{T}^{(2)} = \begin{bmatrix} 0 & 1 & 0 & 0 \\ 1 & 0 & 0 & 0 \\ 0 & 0 & 0 & e^{-j2\pi\frac{1}{2}} \\ 0 & 0 & 1 & 0 \end{bmatrix}$$

That is, channel with one delay circularly shifts the elements in each column (delay dimension) of $\mathbf{s}$ with extra phase shifts.

3) $k_3 = 1, l_3 = 0$*:* In this case, $\mathbf{P}^{(3)}$ becomes $\mathbf{I}_4$ and

$$\mathbf{Q}^{(3)} = \mathbf{T}^{(3)} = \begin{bmatrix} 0 & 0 & 1 & 0 \\ 0 & 0 & 0 & e^{j2\pi\frac{1}{4}} \\ 1 & 0 & 0 & 0 \\ 0 & e^{j2\pi\frac{1}{4}} & 0 & 0 \end{bmatrix}$$

That is, channel with one Doppler circularly shifts the columns (Doppler dimension) of $\mathbf{s}$ with extra phase shifts.

4) $k_4 = 1, l_4 = 1$*:* In this case,

$$\mathbf{T}^{(4)} = \begin{bmatrix} 0 & 0 & 0 & e^{j2\pi\frac{1}{4}} \\ 0 & 0 & 1 & 0 \\ 0 & e^{-j2\pi\frac{1}{4}} & 0 & 0 \\ 1 & 0 & 0 & 0 \end{bmatrix}$$

That is, channel with both delay and Doppler circularly shifts the columns and elements in each column of $\mathbf{s}$.

Remark 1: From [1], [2], [16], the input–output relation for the ideal waveforms case can be written as a 2D convolution in the form

$$\mathbf{Y}(m,n) = \sum_{i=1}^{P} h_i \mathbf{X}([m - l_i]_M, [n - k_i]_N) \tag{30}$$

Therefore, the effective channel matrix in Theorem 1 can be obtained from (30) by replacing h_i with $h_i \alpha_i(m,n)$ ([17]), where the correction factor is given by

$$\alpha_i(m,n) = \begin{cases} e^{-j2\pi\frac{n}{N}} z^{k_i([m-l_i]_M)}, & \text{if } m < l_i \\ z^{k_i([m-l_i]_M)}, & \text{if } m \geq l_i \\ 0, & \text{otherwise.} \end{cases}$$

The extra phase shifts, $\alpha_i(m,n)$, are caused by imperfect bi-orthogonality of the non-ideal waveforms. Note that sparsity of OTFS is not affected by the $\alpha_i(m,n)$'s, hence the complexity of any detection algorithm does not change, when practical waveforms are used.

Based on Theorem 1, we can provide a simplified input–output relation when the waveforms at the transmitter and receiver are arbitrary.

Theorem 2: The effective channel matrix, $\mathbf{H}_{\text{eff}}$ for the arbitrary waveforms can be written as

$$\mathbf{H}_{\text{eff}} = \sum_{i=1}^{P} h_i \left[(\mathbf{I}_N \otimes \mathbf{G}_{\text{rx}})\mathbf{T}^{(i)}(\mathbf{I}_N \otimes \mathbf{G}_{\text{tx}})\right], \tag{31}$$

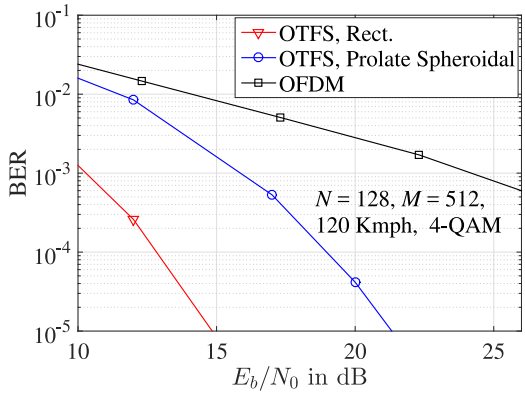

Fig. 1. BER performance of OTFS system with rectangle and prolate spheroidal pulse-shaping waveforms.

Proof: The result can be obtained by writing $\mathbf{H}_{\text{eff}}$ in (11) as

$$\begin{aligned}\mathbf{H}_{\text{eff}} &= (\mathbf{I}_N \otimes \mathbf{G}_{\text{rx}})(\mathbf{F}_N \otimes \mathbf{I}_M)\mathbf{H}(\mathbf{F}_N^{\text{H}} \otimes \mathbf{I}_M)(\mathbf{I}_N \otimes \mathbf{G}_{\text{tx}}) \\ &= (\mathbf{I}_N \otimes \mathbf{G}_{\text{rx}})\mathbf{H}_{\text{eff}}^{\text{rect}}(\mathbf{I}_N \otimes \mathbf{G}_{\text{tx}}) \\ &= (\mathbf{I}_N \otimes \mathbf{G}_{\text{rx}})\left[\sum_{i=1}^{P} h_i \mathbf{T}^{(i)}\right](\mathbf{I}_N \otimes \mathbf{G}_{\text{tx}}) \qquad (32)\end{aligned}$$

Moreover, $\mathbf{H}_{\text{eff}}$ has also exactly P nonzero elements in each row as $(\mathbf{I}_N \otimes \mathbf{G}_{\text{rx}})$ and $(\mathbf{I}_N \otimes \mathbf{G}_{\text{tx}})$ are diagonal matrices. ■

A. A Special Case: Prolate Spheroidal Waveforms

Assume $g_{\text{tx}}(t)$ to be a prolate spheroidal waveform (PSW) [15]: this has a much lower out-of-band power than the rectangular waveform, which reduces the out-of-band interference of OFDM systems. It can be easily shown that an arbitrary $g_{\text{rx}}(t)$ does not affect the performance of maximum likelihood (ML) detection, since both signal and noise components are equally scaled. Therefore, we have selected a rectangular $g_{\text{rx}}(t)$.

Fig. 1 shows the bit error rate (BER) of OTFS vs. E_b/N_0 with rectangular and PSW. This figure also compares OTFS with CP-OFDM as a function of E_b/N_0, where E_b/N_0 takes into account the rate loss of CP-OFDM due to the use of CP overhead. The plot corresponds to the following parameters: carrier frequency = 4 GHz, subcarrier spacing = 15 KHz, $M = 512$, $N = 128$, maximum speed = 120 Kmph, and 4-QAM modulation. We use the Extended Vehicular A model [14] for the channel delay, and each delay tap has a single Doppler shift generated using Jakes' formula $\nu_i = \nu_{\max}\cos(\theta_i)$, where $\nu_{\max}$ is the maximum Doppler shift determined by the UE speed and θ_i is uniformly distributed over $[-\pi, \pi]$. For the detection of transmit symbols, we use the message-passing detector proposed in our earlier work [16], [17]. Note that both waveforms have similar detection complexity, as the sparsity of the effective channel matrix is same.

We can see from the figure that rectangular waveforms outperform by about 5 dB the PSW. This is due to the structure of the latter: here, some of the symbols (edge symbols, see (32)) experience lower channel gains, which degrades the overall performance, while with rectangular waveforms all symbols experience uniform channel gains. Hence, we see a trade-off between out-of-band power and error performance of the OTFS system. Moreover, OTFS with PSW can still be able to outperform OFDM in terms of diversity gain (the BER curve slope).

IV. Conclusion

We have analyzed the input–output relation of OTFS system for arbitrary pulse-shaping waveforms using a block-circulant matrix decomposition. We showed that the OTFS has a simple sparse input-output relation which enables the use of low-complexity detection algorithms. Simulation results, comparing the error performance of OTFS with different waveforms, showed a tradeoff between out-of-band radiation and BER.

References

[1] R. Hadani *et al.*, "Orthogonal time frequency space modulation," in *Proc. IEEE Wireless Commun. Netw. Conf.*, San Francisco, CA, USA, Mar. 2017, pp. 1–6.
[2] R. Hadani *et al.*, "Orthogonal time frequency space modulation." in *Proc. 2017 IEEE Wireless Commun. and Networking Conf. (WCNC)*, Mar. 19–22, 2017, doi: 10.1109/WCNC.2017.7925924
[3] R. Hadani and A. Monk, "OTFS: A new generation of modulation addressing the challenges of 5G," Cohere Technologies, OTFS Phys. White Paper, 7 Feb. 2018. [Online]. Available: https://arxiv.org/abs/1802.02623
[4] A. Fish, S. Gurevich, R. Hadani, A. M. Sayeed, and O. Schwartz, "Delay-Doppler channel estimation in almost linear complexity," *IEEE Trans. Inf. Theory*, vol. 59, no. 11, pp. 7632–7644, Nov. 2013.
[5] Li Li *et al.*, "A simple two-stage equalizer with simplified orthogonal time frequency space modulation over rapidly time-varying channels," unpublished paper, 2017. [Online]. Available: https://arxiv.org/abs/1709.02505
[6] T. Zemen, M. Hofer, and D. Loeschenbrand, "Low-complexity equalization for orthogonal time and frequency signaling (OTFS)," unpublished paper, 2017. [Online]. Available: https://arxiv.org/abs/1710.09916
[7] T. Zemen, M. Hofer, D. Loeschenbrand, and C. Pacher, "Iterative detection for orthogonal precoding in doubly selective channels," in *Proc. 2018 IEEE 29th Annu. Int. Symp.Personal, Indoor and Mobile Radio Commun. (PIMRC)*, Sep. 9–12, 2018, doi: 10.1109/PIMRC.2018.8580716.
[8] A. Farhang, A. RezazadehReyhani, L. E. Doyle, and B. Farhang-Boroujeny, "Low complexity modem structure for OFDM-based orthogonal time frequency space modulation," *IEEE Wireless Commun. Lett.*, vol. 7, no. 3, pp. 344–347, Jun. 2018.
[9] A. RezazadehReyhani, A. Farhang, M. Ji, R. R. Chen, and B. Farhang-Boroujeny, "Analysis of discrete-time MIMO OFDM-based orthogonal time frequency space modulation," in *Proc. IEEE Int. Conf. Commun.*, Kansas City, MO, USA, 2018, pp. 1–6.
[10] H. Bölcskei, P. Duhamel, and R. Hleiss, "Orthogonalization of OFDM/OQAM pulse shaping filters using the discrete Zak transform," *Signal Process.*, vol. 83, pp, 1379–1391, 2003.
[11] G. Durisi, V. I. Morgenshtern, H. Bölcskei, U. G. Schuster, and S. Shamai, (Shitz), "Information theory of underspread WSSUS channels," in *Wireless Communications Over Rapidly Time-Varying Channels*, F. Hlawatsch and G. Matz, Eds. Cambridge, MA, USA: Elsevier, Academic Press, pp. 65–112, 2011, ch. 2.
[12] G. Durisi, U. Schuster, H. Bölcskei, and S. Shamai, "Noncoherent capacity of underspread fading channels," *IEEE Trans. Inf. Theory*, vol. 56, no. 1, pp. 367–395, Jan. 2010.
[13] P. J. Davis, *Circulant Matrices.* New York, NY, USA: Wiley, 1970.
[14] E. Lte, "Evolved universal terrestrial radio access (E-UTRA); base station (BS) radio transmission and reception," ETSI, Sophia Antipolis, France, Tech. Spec., vol. 136, no. 104, p. V8, 3GPP TS 36.104 version 8.6. 0 release 8, Jul. 2009.
[15] D. Slepian, "Prolate spheroidal wave functions, Fourier analysis, and uncertainty — V: The discrete case," *Bell Syst. Tech. J.*, vol. 57, no. 5, pp. 1371–1430, May/Jun. 1978.
[16] P. Raviteja *et al.*, "Low-complexity iterative detection for orthogonal time frequency space modulation," in *Proc. IEEE Wireless Commun. Netw. Conf.*, Barcelona, Apr. 2018, pp. 1–6.
[17] P. Raviteja *et al.*, "Interference cancellation and iterative detection for orthogonal time frequency space modulation," *IEEE Trans. Wireless Commun.*, vol. 17, no. 10, pp. 6501–6515, Oct. 2018, doi: 10.1109/TWC.2018.2860011.